Molecular views of electrokinetic phenomena

D.M. Huang[1], L. Joly[1], C. Cottin-Bizonne[1], C. Ybert[1], E. Trizac[2], L. Bocquet[1]*
[1] LPMCN, UMR CNRS 5586, Université Lyon 1, 69622 Villeurbanne, France
[2] LPTMS, UMR CNRS 8626, Bâtiment 100, Université Paris XI, 91405 Orsay, France

Abstract

The molecular nature of electrokinetic phenomena is examined using molecular dynamics simulations. This allows us to investigate the limitations of the traditional description of these phenomena, which relies on the mean-field Poisson-Boltzmann theory of the electric double layer and continuum hydrodynamics for the flow fields. The emerging molecular picture suggests that continuum hydrodynamics works remarkably well, even down to the nanometer level. However, the macroscopic description of hydrodynamics in terms of the no-slip boundary condition, while valid for wetting surfaces, is shown to break down for non-wetting interfaces, and hydrodynamic slippage at the solid surface is evident. By taking this effect into account in the hydrodynamic picture, accurate predictions of electrokinetic effects can be obtained. In particular hydrodynamic slippage is shown to lead to a significant amplification of the zeta potential relative to the surface electric potential. We also show that, while the Poisson–Boltzmann theory in its most basic form does not reproduce the structure of the electric double layer, suitable modifications to the theory allow both the discrete nature of the fluid and ion specificity to be captured. Anomalous electrokinetic effects, such as non-zero zeta potentials for uncharged surfaces are accordingly reproduced within this framework.

1 INTRODUCTION

The electric double layer (EDL) is a central concept in the understanding of the static and dynamic properties of charged colloidal systems. This notion was introduced in the early works of Gouy, Debye, and Hückel [1] to describe the distribution of microions close to a charged colloidal surface. The EDL width determines the range of electrostatic interactions between macromolecules and therefore controls the static phase behavior of these systems. At the dynamic level, the EDL is at the origin of numerous electrokinetic phenomena [2]: electrophoresis, electro-osmosis, the streaming current or potential, and so on. Because these various effects originate at the *surface* of the sample via the EDL, they provide smart and particularly efficient ways to drive or manipulate flows in microfluidic devices [3], in which surface effects are predominant.

The extent of the EDL is typically on the order of a few nanometers. Electrokinetic phenomena therefore probe the *nanorheology* of the system of solvent and ions at the charged surface. This raises some doubts about the validity of continuum approaches in describing the dynamics at such scales. These doubts are particularly relevant to the traditional description of the EDL dynamics, which relies on both the mean-field Poisson-Boltzmann theory of the microion distributions and continuum hydrodynamics for the flow fields [2]. These two aspects are embodied in the so-called *zeta potential*, denoted ζ, which is *traditionally* defined as the electric potential $V(z_s)$ computed at the surface of shear z_s, where the fluid velocity *vanishes*. This quantity plays a key role in electrokinetic phenomena [2], since it quantifies the coupling between flow characteristics in the solvent (via the mean velocity or applied pressure drop) and electric quantities (the electric field and induced streaming current or potential).

In this article, we investigate using molecular dynamics simulations the limitations of the standard description of electrokinetic phenomena. In section 2, we describe two numerical

---

* E-mail : lyderic.bocquet@univ-lyon1.fr

models: a simple atomic fluid to probe hydrodynamics within the EDL, and a water model to investigate the role of ion specificity. We focus in section 3 on equilibrium properties of charged interfaces. We show that ion distributions in the vicinity of charged interfaces differ from the prediction of the standard Poisson-Boltzmann theory. A modified description is proposed, incorporating as a crucial component an ion-size-dependent hydrophobic solvation energy to account for ion specificity. We then turn to the dynamic behavior and explore in section 4 the influence of interfacial hydrodynamics on electrokinetic effects. We show that the appearance of hydrodynamic slippage[1] at non-wetting surfaces leads to a strong amplification of the zeta potential. Finally, we consider the consequences of deviations from the traditional mean-field theory of the EDL, namely anomalous electrokinetic effects such as non-zero zeta potentials for uncharged surfaces.

2 MODELS

With the aim of investigating electrokinetic phenomena on the molecular level, we have studied by computer simulation two different atomistic fluid systems – a modified Lennard-Jones (LJ) fluid model [4] whose hydrodynamic properties are well understood and the multi-site rigid SPC/E water model [5]. In both cases, the channel through which the fluid was made to flow was also treated at an atomistic level, as two parallel solid substrates comprising fcc lattices of LJ particles whose interactions with the fluid could be tuned to vary surface wettability and to which discrete surface charges could be added to atoms in the top solid layer to simulate uniformly charged surfaces. Dissolved ions were also treated atomistically, as charged LJ atoms.

These models therefore include the discrete nature of the solvent and charges and a tunable wettability of the surface, effects that are usually neglected in the traditional description of electrokinetic phenomena and which are potentially important on the length scale of the EDL. For the LJ fluid model, we chose to describe Coulombic interactions at the level of an effective dielectric medium. This simplifying assumption has enabled us to investigate specifically the generic interplay between hydrodynamic and electrostatic effects. The use of the SPC/E water model, in which water molecules consist of a LJ site and three charged sites representing the oxygen and two hydrogen atoms, has allowed us to go further into the complexity of real systems, by capturing not only the dielectric response of a realistic aqueous system but also its interfacial structure. We stress that despite the relative complexity of these molecular models, we aimed at extracting simple messages from the simulations, which can be useful *in fine* to interpret experiments. Generic models are proposed accordingly, which allow the reported effects to be rationalized quantitatively.

The LJ and SPC/E water fluid models that were studied are explained in detail in Refs. [6] and [7] respectively. Below we discuss the most pertinent features of the two systems.

2.1 A simple atomic fluid: Lennard-Jones model

For the LJ fluid system, a variant of the LJ potential, $v_{ij}(r) = 4\varepsilon[(\sigma/r)^{12} - c_{ij}(\sigma/r)^6]$, with identical interaction energies ε and molecular diameters σ for all particles, was used for inter-particle interactions. The tunable parameter c_{ij} enabled us to adjust the wetting properties of the fluid on the substrate [4]: typical wetting and non-wetting situations were achieved by

---

[1] We stress that the designation '*hydrodynamic slippage*' should not be confused with the terminology '*slip velocity*' commonly used in the electrokinetics literature : while a '*slip velocity*' usually designates the electro-osmotic velocity outside the Debye layer in the electrokinetics literature, '*hydrodynamic slippage*' here refers to a breakdown of the no-slip hydrodynamic boundary condition at the solid surface itself.

taking the fluid-solid cohesivity c_{FS} to be 1 and 0.5 respectively for a fixed fluid-fluid cohesivity $c_{FF} = 1.2$, as measured by contact angles θ of a liquid droplet on the substrate of 80 ° and 140 ° respectively in these two cases for a temperature $k_BT/\varepsilon = 1$ (see Ref [4] for an exhaustive discussion on this point). Charged particles (ions and solid surface atoms) also interacted *via* the Coulomb potential for a medium with dielectric permittivity ε_d: $v_{\alpha\beta}(r) = k_BT$ $q_\alpha q_\beta$ (l_B/r), where q_α and q_β were the interacting charges' valences, $l_B = e^2 /(4\pi\ \varepsilon_d\ k_BT)$ the Bjerrum length ($l_B = \sigma$ for the results below), and e the elementary charge.

The simulated systems were generally made up of 10^4 atoms. A typical solvent density was $\rho_f\sigma^3 \sim 0.9$, while the concentration of ions was varied between $\rho_s\sigma^3 = 5 \times 10^{-3}$ and 0.16, corresponding roughly to an ionic strength between 10^{-2} M and 1 M for a typical value of $\sigma = 0.5$ nm. For $l_B = \sigma$, the corresponding Debye screening length (see below) ranged from a few l_B to a fraction of l_B. Salt-free situations were also investigated. The simulations presented in this article were performed using a charge per unit surface $\Sigma = -0.2e/\sigma^2$. For $\sigma = 0.5$ nm, this translates to a typical surface density of -0.13 C/m^2. For $l_B = \sigma$ and the salt concentrations considered here, the surface potential V_0 ranged between $eV_0 \sim k_BT$ and $eV_0 \sim 4\ k_BT$, allowing us to explore both linear (Debye-Hückel-like) and non-linear situations [2]. In the subsequent analysis, LJ units are used, with a characteristic distance σ and time $\tau = (m\sigma^2/\varepsilon)^{1/2}$.

2.2   Towards realistic models: water

In contrast to the LJ fluid system, for the aqueous system the vacuum permittivity ε_0 was used in the Coulomb potential for the electrostatic interactions instead of the medium's dielectric permittivity ε_d (the motion of the water molecules themselves results in the screening of Coulomb interactions, leading to a bulk dielectric constant of SPC/E water, $\varepsilon_w = \varepsilon_d / \varepsilon_0$, of 68 under ambient conditions [9]). In addition, the standard LJ potential, $v_{ij}(r) = 4\varepsilon_{ij}\ [(\sigma_{ij}/r)^{12} - (\sigma_{ij}/r)^6]$, was used for the aqueous system, together with the Lorentz-Berthelot combining rules, $\sigma_{ij} = (\sigma_{ii} + \sigma_{jj})/2$ and $\varepsilon_{ij} = \sqrt{\varepsilon_{ii}\varepsilon_{jj}}$ for particle types i and j, to obtain the heteronuclear LJ interaction parameters from the homonuclear ones. For the atoms in the solid substrate, LJ parameters were chosen to create, respectively, a hydrophobic and a hydrophilic surface, as characterized by the contact angles of a water droplet on these surfaces of approximately 140 and 55° respectively. Two different alkali halide electrolytes were studied, NaI and NaCl, the only difference we considered between the two cases being anion size (see Ref. [7] for a more complete discussion of the choice of the solid and ion LJ parameters.)

A total of 2160 fluid molecules were used in all cases. Surface charge densities Σ of 0, ±0.031, and ±0.062 C/m^2 and electrolyte concentrations of approximately 0.2 and 1 M were studied. The inter-wall distance was adjusted such that the average pressure, defined by the force per unit area on the solid atoms, was approximately 10 atm in equilibrium simulations, and a constant temperature of 298 K was maintained with a Nosé-Hoover thermostat.

3   STATICS

We now turn to the results of the simulations. We first focus on the equilibrium properties of the charged interfaces. In Fig. 1, we show typical density profiles of the microions close to one of the confining surfaces, in the framework of our simple LJ model. The ions exhibit significant structuration close to the charged surface and thus depart strongly from the simple Poisson-Boltzmann (PB) prediction [1]. However, the oscillations in the ion density profiles

---

[2] We have used the MD code LAMMPS, by S.J. Plimpton [8], available at http://lammps.sandia.gov/.
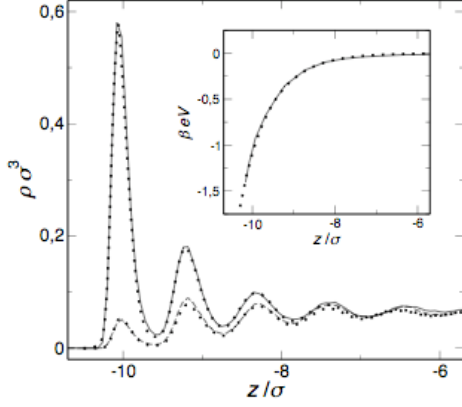
Figure 1: Ion density profiles for the LJ fluid system, averaged over the xy directions ($\rho_s\sigma^3 = 0.06$, $\Sigma = -0.2e/\sigma^2$, $l_B = \sigma$, wetting case). Solid and dashed lines: molecular dynamics results for the counterions (—) and coions (--); dotted lines correspond to the predictions of the modified PB description (see text). The inset shows the electrostatic potential. Solid line: molecular dynamics results calculated from the Poisson equation and the measured ion density profiles; dotted line: bare PB prediction (see text). The position of the wall, defined as that of the centers of the top layer of wall atoms, is located at $z_{wall} = -10.9\sigma$.

originate from the structuration in the solvent itself, which can be captured by a modified PB description,

$$\rho_\pm(z) = \rho_s \exp\left\{-\beta\left[\pm eV(z) + U_{ext}^\pm(z)\right]\right\}, \qquad (1)$$

where $\beta = 1/k_B T$, $V(z)$ is the electrostatic potential, ρ_s is the bulk ion density, and effects other than electrostatic interactions are taken into account through the *effective* external potential $U_{ext}^\pm$. Taking for both cations and anions $U_{ext}^\pm(z) = -k_B T \log\left[\rho_f(z)/\rho_f\right]$, the potential-of-mean-force of a solvent molecule relative to the solid surface, with $\rho_f(z)$ the solvent density profile and ρ_f its bulk value, accounts almost exactly for the discrete nature of the ions (which are identical to the solvent atoms in all respects except electrostatic interactions). Assuming the standard mean-field PB free energy for V then takes care of the electrostatic part [6].

Inserting Eq. (1) and our approximation for $U_{ext}^\pm$ into the Poisson equation gives $\beta e\Delta V = \kappa^2 \gamma(z) \sinh(\beta e\Delta V)$, where $\kappa^{-1} = (8\pi l_B \rho_s)^{-1/2}$ is the Debye screening length defined in terms of the bulk ion concentration, and $\gamma(z) = \rho_f(z)/\rho_f$ is the normalized *solvent* density profile. We tested the accuracy of this approach for calculating $\rho_\pm(z)$, using simulated fluid density profiles, $\rho_f(z)$, as an input. As shown in Fig. 1, this procedure leads to ion density profiles that are in remarkable agreement with the profiles obtained from simulations. Moreover, a further useful approximation can be proposed: the solution of the modified PB equation for the electrostatic potential is in fact very close to the "bare" PB solution $V_{PB}(z)$ (corresponding to $\gamma(z) = 1$), whose analytic expression can be found in the literature [1,2]. This leads to $\rho_\pm(z) \sim \rho_f(z) \exp[\mu\beta e V_{PB}(z)]$. The validity of this approximation - surprising in view of the strong layering effect at work - is emphasized in Fig. 1 (inset), where the corresponding bare PB potential [2] is plotted against the "exact" electrostatic potential. The latter was obtained from the simulations using the Poisson equation by integrating twice the charge density profile $\rho_e = e(\rho_+ - \rho_-)$.

Now turning to the more realistic SPC/E water model, the behavior is more complex than that
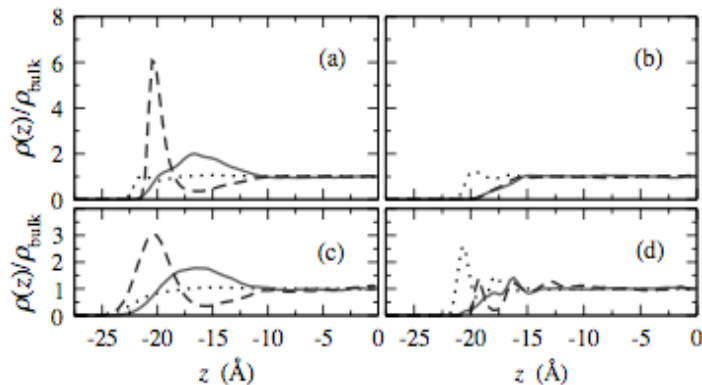

Figure 2: Simulated density profiles (relative to bulk values) of water (dotted lines), positive ions (solid lines), and negative ions (dashed lines) for roughly 1-M aqueous solutions of (a) NaI and (b) NaCl between neutral hydrophobic surfaces, (c) NaI at a water–air interface, and (d) NaI between neutral hydrophilic surfaces.

of the simpler LJ model: Fig. 2 illustrates in particular the dramatic effect anion size and surface wettability can have on interfacial ion densities. While Cl⁻ is not found near the hydrophobic surface in Fig. 2b, Fig. 2a shows a substantially enhanced interfacial I⁻ concentration; in simulations of model anions even larger than I⁻, an even greater enhancement is observed. No such enhancement is seen for I⁻ ions near the hydrophilic surface (Fig. 2c) even though the direct ion-solid interactions are stronger in this case, indicating that the ion density profiles arise largely due to the water structure induced by the surface. The differing behavior of I⁻ and Cl⁻ at hydrophobic and air-water interfaces is at odds with traditional theories of electrolyte interfaces, such as the simple PB model [1], in which ions of the same valency exhibit the same behavior. This ion-specific behavior is also not captured by the modified PB prescription used for the LJ fluid, which assumed ions of equal size. It is known, however, that many interfacial phenomena exhibit a strong dependence on the identity of the cation or anion in solution [10, 11, 12]. One example is the substantial dependence on anion type of the surface tension of aqueous solutions of halide salts [13], which has been explained in terms of differing propensities of the ions for the vapor-liquid interface. Recent spectroscopic experiments [14, 15] and computer simulations [16, 17] have indeed confirmed that the larger bromide and iodide ions exhibit enhanced concentrations at the air-water, in accord with our simulation results, which indicate that iodide ions are attracted by the "vapor-liquid-like" interface induced by a hydrophobic surface [18].

An accurate model for ion densities near aqueous interfaces must therefore account for ion-size-dependent effects and perhaps for the non-uniform non-local dielectric response of water that is known to occur at surfaces [19]. To this end, we used a modified PB approach similar to that employed for the LJ fluid, once again using Eq. (1) but this time solving the general form of the one-dimensional Poisson equation [1] for V with a position-dependent polarization for the medium, $P(z)$,

$$\frac{\mathrm{d}}{\mathrm{d}z}\left[-\epsilon_0 \frac{\mathrm{d}}{\mathrm{d}z}V(z) + P(z)\right] = \rho_\mathrm{e}(z). \qquad (2)$$

Neumann BCs were applied at the position z_wall of the surface charge. A couple of levels of approximation for $P(z)$ were used: the exact value, the gradient of which is equal to minus the charge density due to water in our simulations (we will refer to this as the Full-Polarization (FP) model); and $P(z) = -\epsilon_0 [\varepsilon(z)-1] V'(z)$, where $\varepsilon(z) = \vareps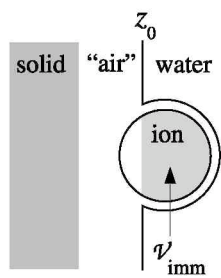ilon_\mathrm{w}$ for $z > z_0$ and 1 for $z < z_0$, with z_0 the position of the first peak in the simulated water oxygen density distribution function (Step-Polarization (SP) model).

In constructing the external potential, our goal was to use the simplest description that accurately captured the physics governing the ion density descriptions. As such, we used $U_\mathrm{ext}^\pm = U_\mathrm{image}^\pm + U_\mathrm{wall}^\pm + U_\mathrm{hyd}^\pm$, the sum of three components: the image charge potential $U_\mathrm{image}^\pm$ acting on ions near the dielectric interface at z_0, as described by the Onsager-Samaras theory [20] (Eq. (3) in [13]); the ion-solid LJ interaction $U_\mathrm{wall}^\pm$, obtained by integrating the truncated and shifted inter-particle LJ interaction over a uniform density ρ_s of solid atoms occupying the half-plane to the left of z_wall; and the hydrophobic solvation energy $U_\mathrm{hyd}^\pm$ to create an ion-sized cavity in the fluid, which we assumed to be proportional to the volume V_imm of the ion immersed in the liquid in the $z > z_0$ half-plane (see Fig. 3) [21]. The constant of proportionality was taken to be the *solvation free energy* per unit volume measured under similar thermodynamic conditions in simulations of hard-sphere solutes of 0–5-Å radius in SPC/E water [21] and the solvent-excluded radius of the ions was taken from bulk simulations of ions in water as the radius at which the ion–water

Figure 3: Schematic of an ion at the solid-liquid interface, illustrating quantities used to calculate $U_\mathrm{hyd}^\pm$

radial distribution function fell to 1/e of its bulk value. This hydrophobic solvation energy has generally been ignored in calculations of ion densities near liquid interfaces, since it is negligible for typical small ions like Na^+ or Cl^-, but it can be significant for larger ions like I^-, as we shall see below.

The total ionic charge density profiles $\rho_e(z)$, calculated using various levels of approximation in Eq. (2) are compared with the simulation results in Fig. 7c and d. Given the simplicity of our model for $U_{ext}^\pm$, the agreement between the theory and simulation is remarkably good. The FP model, in particular, almost exactly reproduces long-range behavior of $\rho_e(z)$, despite some differences with the simulation results in the immediate vicinity of the solid surface. The agreement between theory and simulation is slightly poorer with the simpler SP model, possibly because the dielectric response of water near the surface is non-local and not readily approximated by a local dielectric constant [19].

Unlike the case for the LJ fluid, the electrostatic potential V is not well-approximated by the simple PB formula (i.e. without $U_{ext}^\pm$), due to the observed ion-specific effects. In particular, for an NaI solution between uncharged walls, the surface enhancement of I^- implies a non-zero surface potential, whereas the simple PB theory predicts a vanishing value.

4 DYNAMICS

4.1 Hydrodynamics within the Electric Double Layer

The standard electrokinetic description relies on the assumption of a no-slip boundary condition of the liquid at the solid interface. However, this assumption has been critically revisited in recent years. Indeed, important advances in the rheology of fluids at small scales have been achieved, partly due to computer simulations, such as molecular dynamics (see *e.g.* [4] and refs. therein), but mainly thanks to the development of new experimental techniques, such as optical velocimetry (see [22, 23] and refs. therein) and dissipation measurements using Surface Force Apparatus and Atomic Force Microscope (see [24, 25] and refs. therein). The conclusions emerging from these studies are that, while the continuum hydrodynamics theory surprisingly remains valid *down to very small length scales*, the *no-slip* boundary condition (BC) for the fluid velocity at the solid surface may be violated in many situations (see *e.g.* [4, 24, 25, 26]). Moreover, it has been shown that this violation of the usual no-slip BC is controlled by the wetting properties of the fluid on the solid surface: while the no-slip BC is fulfilled on hydrophilic surfaces, a finite velocity slip is measured on hydrophobic surfaces [4, 24, 26].

We now investigate how interfacial hydrodynamics at the scale of the EDL affects electrokinetic phenomena. We first consider a *streaming current* experiment for the LJ fluid model: an external volume force f_0 is applied to the fluid in the x direction, enforcing a Poiseuille flow in the cell, and the electric current I_e associated with the convective motion of the ions is measured. The standard EDL description of this electrokinetic effect predicts a linear relationship between the current and the force, in the form [2]

$$I_e = -\frac{\varepsilon_d \zeta}{\eta} \mathcal{A} f_0, \qquad (3)$$

where η is the shear viscosity of the fluid and $\mathcal{A}$ the fluid slab cross area. In the simulations, an identical force per particle was applied to each of the fluid particles and the corresponding electric current is measured. Linear response (in the applied force) was carefully checked. In the following we use Eq. (3) as the *definition of the ζ potential*, in line with experimental procedures.
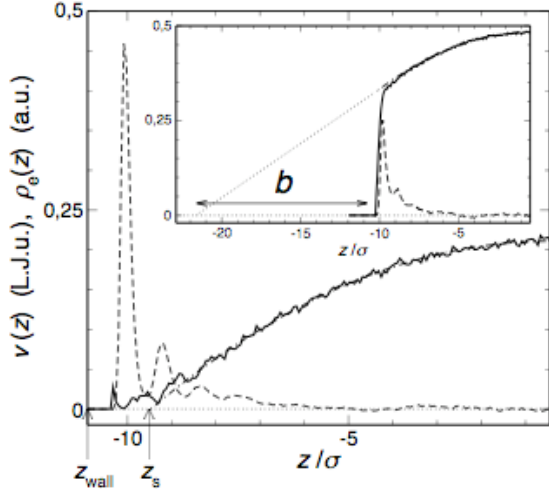
Figure 4: Measured Poiseuille velocity profile (solid line) for the LJ fluid system in the wetting case ($c_{FS} = 1$, $\rho_s\sigma^3 = 0.06$, $\Sigma = - 0.2e/\sigma^2$, $l_B = \sigma$). Dashed-dotted line: hydrodynamic prediction using a no-slip BC at the 'plane of shear' located at z_s (indicated by the arrow). To emphasize the existence of an immobile Stern layer, we also indicate the charge density profile $\rho_e(z) = e(\rho_+(z) - \rho_-(z))$ (dashed line), with arbitrary units. The position of the wall (defined as that of the centers of the top layer of wall atoms) is at $z_{wall} = -10.9\sigma$. Inset: Results for the non-wetting case ($c_{FS} = 0.5$). Solid line: velocity profile measured in the simulation (shown on the same scale as in the main graph); dashed-dotted line: hydrodynamic prediction with a partial slip BC, with a slip length $b \sim 11\sigma$; dashed line: charge density profile (arbitrary units).

We start by discussing the measured velocity profiles. A typical situation corresponding to a wetting substrate – with $c_{FS} = 1$ in the LJ model – is shown in the main plot of Fig. 4 (here for $f_0 = 0.02$ in LJ units). The velocity profile shows a parabolic shape as predicted by continuum hydrodynamics, even at the EDL level. Moreover, the viscosity, deduced from the curvature of the parabolic shape, retains its bulk value. Nevertheless, our measurements have shown that the no-slip BC applies inside the liquid, *at a distance of about one layer of solvent particles*. This observation is consistent with previous theoretical predictions [4]. This position of the no-slip BC here defines the "plane of shear" position, z_s usually introduced in the electrokinetic literature [2]. We note that z_s does not vary significantly with the salt concentration, in the parameter range investigated. As shown in Fig. 4, where the charge density profile, $\rho_e(z)$, is plotted against distance, the first layer of ions, located within z_s, does not contribute to the convective transport, thereby reducing the global streaming current. This first layer coincides with the so-called Stern layer of immobile ions close to the charged surface [2].

On the other hand, the non-wetting case displays a very different behavior, as shown in the inset of Fig. 4. A non-wetting substrate was set up by choosing a smaller value of c_{FS}, here $c_{FS} = 0.5$. First, concerning the velocity profile, a large amount of slip was found at the wall surface, in accordance with observations on non-wetting surfaces [4]. More quantitatively, slippage is characterized by a *slip length, b,* defined as the distance at which the linear extrapolation of the velocity profile vanishes. In other words, this amounts to replacing the no-slip BC by a partial slip BC, defined as $b\partial_z v = v$ at the wall position [4]. As shown in the inset of Fig. 4, the velocity profile is well fitted by the continuum hydrodynamics (parabolic) prediction, together with a partial slip BC, characterized by a non-vanishing slip length (here $b \sim 11\sigma$). The measured slip length b hardly depends on the salt concentration. Concerning microion transport, an important point here is that the first layer of ions now contributes to a large extent to the global streaming current, in contrast with the wetting case. In other words, the plane of shear position z_s is now located at a virtual position *beyond* the wall and the Stern layer has completely disappeared. The remobilization of the Stern layer adds to the slippage effect and contributes significantly to the increase of the electric current measured for hydrophobic surfaces.

4.2 Zeta potential

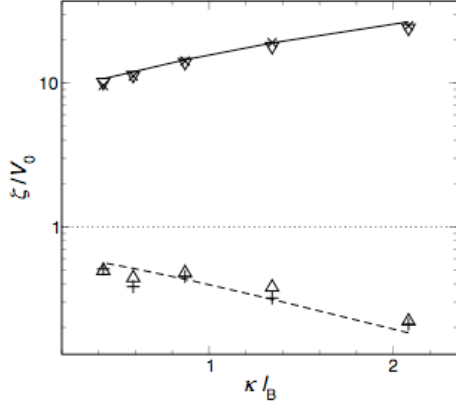We summarize our results for the LJ fluid system in Fig. 5 and plot the ζ potential

Figure 5: Measured ζ potential for the LJ fluid system as a function of the screening factor $\kappa\, l_B$ in streaming current (triangle up: wetting case; triangle down: non-wetting case) and electro-osmosis (plus: wetting case; cross: non-wetting case) simulations. The ζ potential is normalized by the bare surface potential V_0 obtained from the PB expression at a given κ and surface charge (see the discussion on the inset of Fig. 1). For the wetting case (bottom), the dashed line is the PB electrostatic potential $V(z_s)$, where the 'plane of shear' position z_s does not vary significantly with salt. For the non-wetting case (top), the solid line corresponds to the slip prediction Eq. (5), with $b = 11\sigma$.

(determined from the measurement of the charge current and Eq. (3)) as a function of the Debye screening factor in the wetting and non-wetting cases. In this figure the ζ potential is normalized by the bare surface potential V_0, obtained from the analytic PB expression [2], as shown *e.g.* in the inset of Fig. 1. The overall conclusion from Fig. 5 is that non-wettability strongly amplifies the electrokinetic effects: the ratio between the ζ potential and the surface potential is much larger in the hydrophobic case than in the hydrophilic case. More precisely, in the wetting case the ζ potential is fixed by the electric properties of the surface, and coincides with the electric potential at the "plane of shear", $\zeta \sim V(z_s)$, as is usually assumed [2]. Indeed, the simulation points for ζ correspond closely with the PB estimate for the electric potential $V(z_s)$. Conversely, the ζ potential in the non-wetting case is dominated by the slip effect and the immobile Stern layer is completely absent. The effect of such a modification of the hydrodynamic surface properties can be accounted for by considering the partial slip BC in the electrokinetic current $I_e = \int dS\, \rho_e(z)v(z)$, with $\rho_e(z)$ the charge density and $v(z)$ the velocity profile, characterized by a slip length b. Within the linearized PB description (valid for $eV_0 << k_BT$), the result for the current I_e, Eq. (3), may then be written as $I_e = (\varepsilon_d V_0/\eta)(1 + \kappa b)f_0$ [3, 27]. For the ζ potential in the non-wetting case, this amounts to

$$\zeta = V_0(1 + \kappa b), \qquad (4)$$

with V_0 the bare potential of the surface. A detailed derivation of this effect is given in [6].

For large potentials ($eV_0 > k_BT$), a non-linear PB counterpart of this expression can be obtained [6]:

$$\zeta = V_0(1 + \kappa_{\text{eff}} b), \qquad (5)$$

where the effective Debye length κ_{eff}^{-1} is defined by $\kappa_{\text{eff}} = -\partial_n V(0)/V_0$, and goes to κ^{-1} in the linear limit. An equivalent expression has been recently discussed in a molecular hydrodynamics study of electro-osmosis in clays [28]. This expression is compared with simulation results in Fig. 5, showing again very good agreement.

The streaming current simulations show that electrokinetic measurements do not probe electrostatic properties of the system only: when slippage occurs at the walls, the ζ potential is much larger than the bare surface potential V_0. This also means that the electrokinetic phenomena used to move liquids in microfluidic systems could be strongly amplified by hydrodynamic slippage. In order to illustrate this interesting possibility, we performed electro-osmosis simulations, using the same LJ fluid system. A uniform electric field E_x applied in the channel induces a volume force inside the EDL, generating as a result a plug flow of the liquid. The standard description of this phenomenon predicts again a linear relationship between the electro-osmotic velocity and the applied field:

$$v_{\mathrm{eo}} = -(\varepsilon_{\mathrm{d}}\zeta/\eta)E_x. \quad (6)$$

In the simulation, we imposed an electric force $f_x = qeE_x$ to every ion *(qe* being the ion charge), and we measured the resulting velocity profile in the channel. We then used Eq. (6) to compute the corresponding ζ potential (the results presented were obtained for $E_x = 1.0$ in LJ units). As for the streaming current, linear response in the applied electric field was
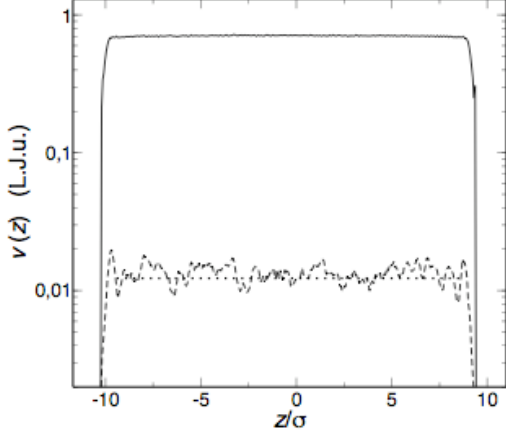

Figure 6: Solvent velocity profile *v(z)* for the LJ system, averaged over the *xy* directions, in a typical electro-osmosis simulation ($\rho_s\sigma^3 = 0.06$). An electric field E_x was applied along the *x* direction, leading to a plug velocity profile in the cell. The dashed line corresponds to the wetting case ($c_{\mathrm{FS}} = 1$), whereas the solid line corresponds to the non-wetting case ($c_{\mathrm{FS}} = 0.5$). The Debye screening factor was $\kappa\, l_{\mathrm{B}} = 1.3$.

checked.

Typical velocity profiles are shown in Fig. 6. For both wetting and non-wetting situations, we observe a plug flow, characteristic of electro-osmosis. Moreover, we note that the electro-osmotic velocity is considerably amplified - by almost two orders of magnitude - in the non-wetting case, all electrical parameters being equal. The ζ potentials, computed from the measured electro-osmotic velocity using Eq. (6), are in perfect agreement with those obtained in streaming current simulations, as can be seen on Fig. 5.

4.3   Ion-specific electrokinetics

Electrokinetics in water exhibits many of the general features observed for the LJ fluid, but as we shall demonstrate below, the aqueous system has additional characteristics not encountered with the simpler model, most notably associated with the ion specificity that was encountered earlier for the interfacial fluid structure.
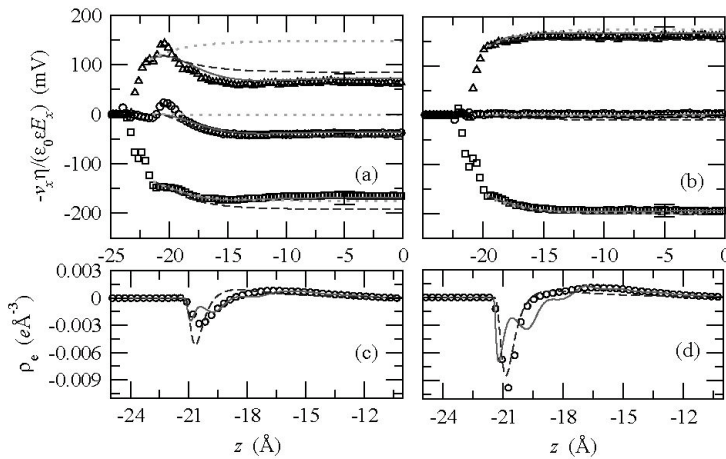

Figure 7: *Top*: Velocity profiles in a hydrophobic channel for $\Sigma = -0.062$, 0, and $+0.062$ C/m^2 (from bottom to top) with (a) [NaI] ≈ 1 M and (b) [NaCl] ≈ 1 M. The simulation results (symbols) are compared with solutions of the modified PB equation using (see text for details) the FP model (solid lines), the SP model (dashed lines), and the SP model with $U_{\mathrm{hyd}}^{\pm} = 0$ (dotted lines). Typical error bars for the theoretical curves are shown. Error bars in the simulated velocities are roughly the size of the points. *Bottom*: Ionic charge density profile $\rho_e(z)$ for [NaI] ≈ 1 M with (c) $\Sigma = 0$ and (d) $\Sigma = +0.062$ C/m^2. The symbols are from simulation. The solid and dashed lines are solutions of the modified PB equation with the FP and SP models respectively.

9

In the water simulations, electro-osmotic flow was induced by applying an electric field E_x in the x direction (linear response to the applied field was verified). The measured velocity $v_x(z)$ is shown in Fig. 7 for the 1-M solutions with $\Sigma = 0$ and ± 0.062 C/m^2; $v_x(z)$ has been scaled by η, E_x and the bulk dielectric constant $\varepsilon_w = 68$ of pure SPC/E water [9], for ease of comparison with the ζ potential, defined in (6), where v_{eo} was taken as the velocity in the channel center. The zeta potentials for all the surface charges and concentrations are given in Fig. 8.

Figures 7 and 8 clearly show the sensitivity of the EO flow to anion type, particularly for the neutral and positively charged surfaces. (The flow for the negatively charged surfaces is dominated by the excess of cations, which was Na$^+$ in all simulations.) Contrary to the traditional theory of the EDL [1], but as observed in previous experiments [29, 30] and computer simulations [31], a non-zero ζ potential was measured for the 1-M NaI solutions in the neutral hydrophobic channel, even though the total electrostatic force exerted on the charge-neutral fluid is zero. By contrast, ζ for NaCl in the same channel was negligible. Our measured ζ potentials of 0 and -38 mV respectively for 1-M NaCl and NaI are consistent with experimental surface potentials of roughly 0 and -20 mV respectively for vapor–liquid interfaces of the same solutions [32]; ζ for NaI is also of similar magnitude to the value of -9 mV measured by electrophoresis of neutral liposomes in 1 M KI [30], for which ion-specific effects should be smaller due to the greater similarity in size of K$^+$ and I$^-$ compared with Na$^+$ and I$^-$. Although not shown in Fig. 7, ζ was insignificant for NaI in the neutral hydrophilic channel. The non-monotonic behavior of ζ as a function of Σ in Fig. 8, which is contrary to the predictions of the conventional theory of electro-osmosis with non-slip BCs [2], is due to the decrease in fluid slip at the surface with Σ (see [6,7] for detailed explanations). Figure 8b shows a weak dependence of ζ on salt concentration for the small number of cases studied, as was observed for the LJ fluid.

Despite the presence of ion-specific electrokinetic effects for the aqueous systems studied, just as with the simpler LJ system, the flow profiles can be quantitatively predicted using
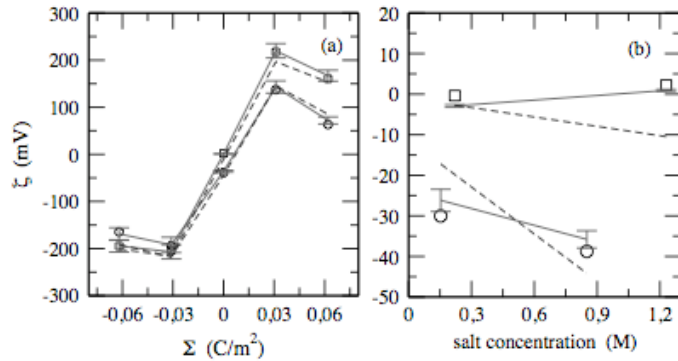

Figure 8: Zeta potential of hydrophobic channels versus (a) surface charge for 1 M aqueous solutions of NaI and NaCl and (b) salt concentration for NaI and NaCl with $\Sigma = 0$ (simulation: NaI – circles; NaCl – squares). The lines are solutions of the Stokes equation with ρ_e from solving PB equation using the Full-Polarization (solid) and Step-Polarization (dashed) models (see text). Typical error bars for the theoretical curves are shown. Error bars in the simulated ζ are roughly the size of the points.

continuum hydrodynamics, in which the EO flow is described by the Stokes equation [2], $\partial_{zz}v_x(z) = -(E_x/\eta)\,\rho_e(z)$. Integrating the Stokes equation twice with boundary conditions (BCs) $v_x(z=z_h) = b\,\partial_z v_x(z=z_h)$ and $\partial_z v_x(z=0) = 0$, where b is the slip length, gives for a system symmetric about $z = 0$

$$\zeta \equiv -\frac{\eta v_x(0)}{\epsilon_0 \epsilon_w E_x} = -\frac{1}{\epsilon_0 \epsilon_w}\int_{z_h}^{0} dz'(z' - z_h + b)\rho_e(z'). \quad (7)$$

This general equation makes no assumptions about the functional form of $\rho_e(z)$. If, however, we substitute the Poisson equation, $-\epsilon_0 \epsilon_w V''(z) = \rho_e$, with non-varying dielectric permittivity, $\varepsilon_d = \epsilon_0 \epsilon_w$, into Eq. (7), we recover the analytical result, Eq. (5), for the slip-induced

amplification of ζ that was found to be quantitatively accurate for the LJ fluid. Solving the Stokes equation using values of b and η measured independently from Couette and Poiseuille flow simulations respectively and the exact ρ_e from our simulations, we also found almost perfect agreement with the simulated velocity profiles and ζ potentials shown in Figs. 7 and 8 (not shown), confirming the accuracy of the continuum hydrodynamic picture even for the more complex water solvent.

 Equation (7) also explains in general terms the anomalous ion-specific electrokinetic effects observed for water. According to Eq. (7), ζ is proportional to the *first moment* of the charge distribution ρ_e relative to an origin at the shear plane, $z_s = z_h - b$. Unless $\rho_e(z) = 0$ everywhere, this quantity will generally be non-zero even if the total charge, $\int_{z_s}^{0} dz' \rho_e(z')$, is zero, as is the case for NaI near the uncharged hydrophobic wall due to the differing propensities of Na$^+$ and I$^-$ for the surface. Although it has been suggested that a non-zero ζ potential occurs for some non-charged surfaces due to ion-specific "binding" [30] or the presence of an immobile interfacial layer of charge [29], our results show that ζ will be nonzero even if all of the charge is mobile. Another interesting consequence of Eq. (7) is that, as long as b is finite, surface slippage makes no contribution to the velocity of a charge-neutral fluid containing only mobile charge: *i.e.* the system behaves as if $b = 0$ and the flow is independent of the solid-fluid friction. If b is infinite, this condition no longer holds and the velocity at z_h is determined by momentum conservation, as momentum cannot be transferred to a frictionless surface. For the condition of zero total momentum used in our simulations, the velocity in the channel center in this case would go to zero as the inter-wall separation tended to infinity.

Using charge density profiles ρ_e calculated from the modified PB model as input into the Stokes equation provides a means of quantifying ion-specific electrokinetic effects from first principles. The flow profiles and zeta potentials calculated from ρ_e obtained with the FP and SP models are shown in Figs. 7 and 8 respectively. It can be seen that the agreement between theory and simulation is very good is both cases, despite the simplicity of the models, and with the Full-Polarization model the accord is almost perfect. On the other hand, if the hydrophobic solvation free energy $U_{hyd}^{\pm}$ is left out, I$^-$ ions display no preference for the interface compared with Na$^+$ and both the calculated ion density profiles and velocities are significantly wrong for the neutral and positively charged surfaces. For the negatively charged surfaces, the flow is dominated by Na$^+$, for which $U_{hyd}^{\pm}$ is negligible. Similarly, the discrepancy between the theory and simulations is smaller for NaCl as $U_{hyd}^{\pm}$ makes a small contribution for these ions. Although not shown, we found that the conventional theory of the electric double layer, which assumes $\varepsilon(z) = \varepsilon_w$ and $U_{ext}^{\pm} = 0$ everywhere, works very poorly in almost all cases. In particular, this simple theory makes the unphysical prediction of finite ion density all the way up to the first layer of solid atoms, leading to almost no mobile charge and a substantial under-prediction of the fluid velocity.

5   CONCLUSIONS

Using molecular dynamics simulations, we have investigated the limitations of the traditional description of electrokinetic phenomena, which relies on both the mean-field Poisson-Boltzmann theory of the electric double layer and continuum hydrodynamics for the flow fields. Two main deviations from macroscopic theories that are of molecular origin were demonstrated.

On one hand, we have addressed the consequences of hydrodynamic slippage on electrokinetic phenomena, through the coupling between hydrodynamics and electric charge

within the electric double layer. We have shown that the widely used "zeta potential" -which characterizes the amplitude of electrokinetic effects- is not only a signature of interfacial electrostatic features, but is also intrinsically related to the dynamics of the solvent at the solid surface, thus providing new perspectives to control this quantity. A similar conclusion was reached in recent work [28]. In particular, we have demonstrated the existence of strongly amplified electro-osmotic effects on hydrophobic surfaces through the induced slippage, in quantitative agreement with previous streaming current simulations. Furthermore, the simulation results have been shown to be in excellent agreement with continuum hydrodynamic predictions that took into account the slippage of the fluid at the solid surface. The amplification effect is accordingly controlled by the ratio between the slip length (of the fluid at the solid surface), and the Debye length, i.e. the width of the EDL.

On the other hand, we have shown that anomalous electrokinetic effects occur quite generally for electro-osmosis flow of aqueous solutions in hydrophobic channels when the dissolved cation and anion differ substantially in size. This behavior is due to the stronger attraction of larger ions to the "vapor-liquid-like" interface induced by a hydrophobic surface. We have also developed a simple model, comprising continuum hydrodynamic equations and a modified Poisson-Boltzmann description for the ion densities, which accurately predicts the simulated flow profiles. We have found that the incorporation in the model of an ion-size-dependent hydrophobic solvation energy, which favors interfacial enhancement of large ions, is crucial to reproducing the ion-specific effects observed in the simulations. Such an analytical theory, which is able to capture the subtle and complex effects of the interfacial specificity of ions, provides a very useful framework for the modeling of biological systems.

References

1. Lyklema, J., 1995, Fundamentals of interface and colloid science, vol. 2, Academic Press, London.
2. Hunter, R.J., 1981, Zeta potential in colloid science, Academic Press, London.
3. Stone, H.A., Stroock, A., and Ajdari, A., 2004, Annu. Rev. Fluid Mech., 36, 381.
4. Barrat, J.L. and Bocquet, L., 1999, Phys. Rev. Lett., 82, 4671.
5. Berendsen, H.J.C., Grigera, J.R., and Straatsma, T.P., 1987, J. Phys. Chem., 91, 6269.
6. Joly, L., Ybert, C., Trizac, E., and Bocquet, L., 2006, J. Chem. Phys., 125, 204716.
7. Huang, D.M., Cottin-Bizonne, C., Ybert, C., and Bocquet, L., 2007, Phys. Rev. Lett., 98, 177801.
8. Plimpton, S.J., 1995, J. Comput. Phys., 117, 1.
9. Höchtl, P., Boresch, S., Bitomsky, W., and Steinhauser, O., 1998, J. Chem. Phys., 109, 4927.
10. Kunz, W., Lo Nostro, P., and Ninham, B.W., 2004, Curr. Opin. Colloid Interface Sci., 9, 1.
11. Jungwirth, P. and Tobias, D.J., 2006, Chem. Rev., 106, 1259.
12. Cacace, M.G., Landau, E.M., and Ramsden, J.J., 1997, Q. Rev. Biophys., 30, 241.
13. Boström, M., Kunz, W., and Ninham, B.W., 2005, Langmuir, 21, 2619.
14. Ghosal, S., Hemminger, J.C., Bluhm, H., Mun, B.S., Hebenstreit, E.L.D., Ketteler, G., Ogletree, D.F., Requejo, F.G., and Salmeron, M., 2005, Science, 307, 563.
15. Petersen, P.B., Johnson, J.C., Knutsen, K.P., and Saykally, R.J., 2004, Chem. Phys. Lett., 397, 46.
16. Vrbka, L., Mucha, M., Minofar, B., Jungwirth, P., Brown, E.C., and Tobias, D.J., 2004, Curr. Opin. Colloid Interface Sci., 9, 67.
17. Archontis, G., Leontidis, E., and Andreou, G., 2005, J. Phys. Chem. B, 109, 17957.
18. Huang, D.M. and Chandler, D., 2002, J. Phys. Chem. B, 106, 2047.
19. Faraudo, J. and Bresme, F., 2004, Phys. Rev. Lett., 92, 236102.
20. Onsager, L. and Samaras, N.N.T., 1934, J. Chem. Phys., 2, 528.
21. Huang, D.M., , Geissler, P.L., and Chandler, D., 2001, J. Phys. Chem. B, 105, 6704.
22. Joseph, P. and Tabeling, P., 2005, Phys. Rev. E, 71, 035303.
23. Schmatko, T., Hervet, H., and Léger, L., 2005, Phys. Rev. Lett., 94, 244501.
24. Cottin-Bizonne, C., Cross, B., Steinberger, A., and Charlaix, E., 2005, Phys. Rev. Lett., 94, 056102.

25. Vinogradova, O.I. and Yakubov, G.E., 2006, Phys. Rev. E, 73, 045302.

26. Joly, L., Ybert, C., and Bocquet, L., 2006, Phys. Rev. Lett., 96, 046101.

27. Churaev, N.V., Ralston, J., Sergeeva, I.P., and Sobolev, V.D., 2002, Adv. Colloid Interface Sci., 96, 265.

28. Dufrêche, J.F., Marry, V., Malikova, N., and Turq, P., 2005, J. Mol. Liq., 118, 145.

29. Dukhin, A., Dukhin, S., and Goetz, P., 2005, Langmuir, 21, 9990.

30. Petrache, H.I., Zemb, T., Belloni, L., and Parsegian, V.A., 2006, Proc. Natl. Acad. Sci. USA, 103, 7982.

31. Joseph, S. and Aluru, N.R., 2006, Langmuir, 22, 9041.

32. Jarvis, N.L. and Scheiman, M.A., 1968, J. Phys. Chem., 72, 74.